

# Journal of Biomedical Optics

BiomedicalOptics.SPIEDigitalLibrary.org

## **Velocity measurements of heterogeneous RBC flow in capillary vessels using dynamic laser speckle signal**

Chenxi Li  
Ruikang Wang

**SPIE.**

Chenxi Li, Ruikang Wang, "Velocity measurements of heterogeneous RBC flow in capillary vessels using dynamic laser speckle signal," *J. Biomed. Opt.* **22**(4), 046002 (2017), doi: 10.1117/1.JBO.22.4.046002.

# Velocity measurements of heterogeneous RBC flow in capillary vessels using dynamic laser speckle signal

Chenxi Li<sup>a,b</sup> and Ruikang Wang<sup>a,b,\*</sup>

<sup>a</sup>University of Washington, Department of Bioengineering, Seattle, Washington, United States

<sup>b</sup>Tianjin University, College of Precision Instrument and Optoelectronics Engineering, Tianjin, China

**Abstract.** We propose an approach to measure heterogeneous velocities of red blood cells (RBCs) in capillary vessels using full-field time-varying dynamic speckle signals. The approach utilizes a low coherent laser speckle imaging system to record the instantaneous speckle pattern, followed by an eigen-decomposition-based filtering algorithm to extract dynamic speckle signal due to the moving RBCs. The velocity of heterogeneous RBC flows is determined by cross-correlating the temporal dynamic speckle signals obtained at adjacent locations. We verify the approach by imaging mouse pinna *in vivo*, demonstrating its capability for full-field RBC flow mapping and quantifying flow pattern with high resolution. It is expected to investigate the dynamic action of RBCs flow in capillaries under physiological changes. © 2017 Society of Photo-Optical Instrumentation Engineers (SPIE) [DOI: 10.1117/1.JBO.22.4.046002]

Keywords: laser speckle; heterogeneous RBC flow; eigen-decomposition; cross-correlation; velocity.

Paper 170100LR received Feb. 14, 2017; accepted for publication Mar. 21, 2017; published online Apr. 6, 2017.

## 1 Introduction

An ability to quantitate the velocity of red blood cells (RBCs) in capillary vessels is critical for understanding the dynamic actions of microvascular adaptation to their environment, including physiological changes.<sup>1–3</sup> Many optical methods have been developed to measure blood flow, including Doppler-based methods (e.g., laser Doppler flowmetry, Doppler optical coherent tomography, and photoacoustic Doppler),<sup>4–6</sup> RBC-tracking measurements [e.g., multiphoton laser scanning microscopy (MPLSM), retinal function imager (RFI)],<sup>7,8</sup> and laser speckle contrast imaging (LSCI).<sup>9</sup> Doppler-based methods require a prior knowledge of Doppler angle to recover axial velocity components. MPLSM tracks the fluorescently labeled RBCs with high spatial resolution; however, its field of view is severely limited, typically confined to one microvessel at a time, and the fluorescent dye is susceptible to photobleaching. RFI achieves wide-field imaging of blood flow velocity with intrinsic optical signal of RBCs, but its signal–noise ratio (SNR) is low and the measurement is typically confined to the surface blood vessels. By the use of raster scanning of a focused beam spot, several methods based on cross-correlation or autocorrelation have been demonstrated in the fields of photoacoustic imaging and optical coherence tomography to measure velocity of capillary flow.<sup>10,11</sup> Although promising, these methods typically compromise the system useful capabilities due to the coupled relationship among imaging speed, field of view, and resolution during practical imaging. Taking the advantages of wide field imaging, simple system setup, and cost-effectiveness, LSCI is a powerful tool for qualitative assessment of tissue blood perfusion. With the statistical model established by Fercher, the metric of speckle contrast defined as the ratio of the standard deviation to the mean value of speckle intensity is mostly used.<sup>9</sup> So far, the LSCI method is not amenable to measuring the RBC flows

in individual capillaries, which are single files and often heterogeneous in both spatial and temporal dimensions.

In this letter, we demonstrate a cross-correlation-based approach to measure the velocity of heterogeneous RBC flows using full-field time-varying dynamic speckle signals captured by a low coherent laser speckle imaging system. To eliminate the effect of static tissue components on the analyses of dynamic flow signals, we propose using an eigen-decomposition filtering (ED-filtering) algorithm to extract the dynamic speckle signal due to the moving RBCs, through which a full-field dynamic RBC flow mapping with high spatial and temporal resolution is achieved.<sup>12</sup> The transit time ( $\tau$ ) of RBC flow in one capillary is calculated with the cross-correlation function of the two time-varying dynamic speckle signals obtained at adjacent locations (with a short distance of  $L$ ). Then, the RBCs flow velocity ( $v$ ) is determined through  $v = L/\tau$ .

## 2 Method

### 2.1 Dynamic RBC Signal Extraction with ED-Filtering Algorithm

The coherent light scattered by the blood perfused tissue produces speckle pattern. The tissue components give speckle pattern that is often static, while flowing RBCs give rise to spatial and temporal fluctuations of the speckle pattern. Assuming that the static speckle signal arises from a low dimensional space (with low frequency) and the dynamic signal arises from high dimension (with high frequency), the separation of dynamic speckle signal from static speckle signal could be achieved by dimensional a reduction method such as eigen-decomposition.<sup>12,13</sup>

In an LSCI system, we assume that a series of raw speckle frames with two spatial dimensions ( $M = P \times Q$  pixel array) and one temporal dimension ( $N$  frames) are captured by the camera. Then, the raw signals could be reshaped in one

\*Address all correspondence to: Ruikang Wang, E-mail: wangrk@uw.edu

spatiotemporal representation (Casorati matrix), where all pixels at the same time point are arranged in one column, and all time points for one pixel are arranged in one row. Viewed from the time dimension, the raw signals would consist of static tissue signal, dynamic RBCs signal, and random white noise. Mathematically, it can be expressed as

$$\mathbf{X} = [\mathbf{x}_1, \mathbf{x}_2, \dots, \mathbf{x}_n]^T = \mathbf{X}_S + \mathbf{X}_B + \mathbf{X}_W, \quad (1)$$

where the superscript  $T$  denotes matrix transposition.  $\mathbf{x}$  is a one-dimensional vector with the length of  $M$ , representing the  $i$ 'th snapshot of temporal speckle signal.  $\mathbf{X}_S$ ,  $\mathbf{X}_B$ , and  $\mathbf{X}_W$  are the matrices (with size of  $M \times N$ ) of the static tissue signal, dynamic RBCs signal, and white noise, respectively. Assuming that there is no correlation between  $\mathbf{X}_B$  and  $\mathbf{X}_S + \mathbf{X}_W$ , from a vector space perspective, the separation of  $\mathbf{X}_B$  from  $\mathbf{X}$  can be determined by an ED-filtering algorithm, previous literature.<sup>12-14</sup>

Because the volume fraction of RBCs within tissue is only  $\sim 2\%$  to  $3\%$ , the power of dynamic RBCs signal would be much smaller than that of the static tissue signal for the area of interest. In particular, assuming there are  $P$  eigenvectors corresponding to the static tissue signal, then the filtering procedure could be achieved via a linear regression strategy that computes the fitting residual between the tissue signal's eigenvector and the raw speckle signal  $\mathbf{X}$  as follow:

$$\mathbf{X}_B = \left(1 - \sum_{i=1}^P \mathbf{e}_i \mathbf{e}_i^T\right) \cdot \mathbf{X}, \quad (2)$$

where  $\mathbf{e}_i$  is the  $i$ 'th eigenvector of  $\mathbf{X}$ . In the experiments described below,  $N$  and  $P$  are optimized to be 4 and 2, respectively, to achieve satisfactory SNR and temporal resolution.  $\mathbf{X}_B$  is finally normalized toward  $\mathbf{X}_S$ , to eliminate the uneven laser intensity distribution over the imaged area, leading to enhanced contrast of dynamic speckle signal.

## 2.2 Cross-Correlation Method

Consider that there are two time-varying dynamic speckle signals  $\mathbf{Y}_B(\mathbf{t})$  and  $\mathbf{Z}_B(\mathbf{t})$  at two locations of  $Y$  and  $Z$  in one capillary obtained using the method described above. When the same group of RBCs travels from  $Y$  to  $Z$ , the time series of signal  $\mathbf{Z}_B(\mathbf{t})$  would appear as an identical copy of  $\mathbf{Y}_B(\mathbf{t})$  but with a time lag of  $\tau$ . Then, it would be trivial that the cross-correlation function  $r_{xy}(\mathbf{k})$  can be used to determine the time delay between  $\mathbf{Y}_B(\mathbf{t})$  and  $\mathbf{Z}_B(\mathbf{t})$

$$r_{xy}(\mathbf{k}) = \frac{\sum_{t=1-k}^{N-k} [\mathbf{Y}_B(\mathbf{t}) - \overline{\mathbf{Y}_B(\mathbf{t})}] [\mathbf{Z}_B(\mathbf{t}+\mathbf{k}) - \overline{\mathbf{Z}_B(\mathbf{t})}]}{\sqrt{\sum_{t=1-k}^{N-k} [\mathbf{Y}_B(\mathbf{t}) - \overline{\mathbf{Y}_B(\mathbf{t})}]^2 \sum_{t=1-k}^{N-k} [\mathbf{Z}_B(\mathbf{t}) - \overline{\mathbf{Z}_B(\mathbf{t})}]^2}}, \quad (3)$$

$$\tau = \max_k [r_{xy}(k)]. \quad (4)$$

## 2.3 Laser Speckle Imaging System

To demonstrate this approach, we developed a simple laser speckle imaging system as shown in Fig. 1. A collimated beam from a low coherent laser emitted diode ( $\lambda = 530 \pm 20$  nm,  $2\text{-}\mu\text{m}$  coherent length,  $30\text{-mW}$  output power, and stability of  $0.2\%$  within 1 min) was expanded to illuminate the sample.

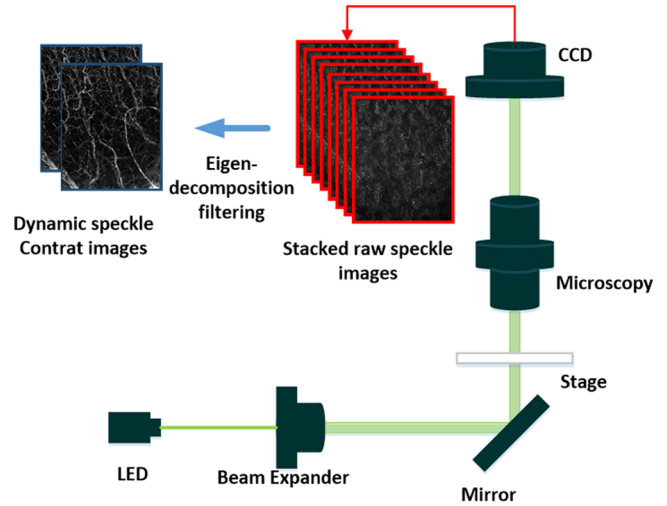


**Fig. 1** Schematic of the laser speckle imaging system. ED-based filtering algorithm is applied to adjacent  $N$  ensemble frames throughout all the raw speckle images.

Then, the diffuse transmitted light through the tissue was collected by a microscope and relayed onto a CCD camera ( $1280 \times 1024$  pixels, pixel size  $12 \mu\text{m} \times 12 \mu\text{m}$ , Basler A504k, Germany). The magnification was adjusted to be  $9\times$  to meet the requirement of sampling the dynamic speckle pattern of single flowing RBC,<sup>15</sup> providing a field view of  $1.71 \text{ mm} \times 1.37 \text{ mm}$  and a spatial resolution of  $1.2 \mu\text{m}$  (pixel-to-pixel spacing). The speckle fluctuation was captured with a  $1\text{-ms}$  exposure period and  $500\text{-frames per second}$  sampling rate. The mouse pinna was chosen to demonstrate the visualization and quantitation of the velocities of RBC flows in capillaries. During the experiment, the animal was anesthetized and carefully handled in accordance with the laboratory animal protocol approved by the University of Washington Institutional Animal Care and Use Committee.

The interference speckle pattern takes place between the scattered light following a similar path that is less than the coherent length. With a low coherent light source, the spatial resolution and imaging contrast would be improved by reducing the contribution of multiple scattering photons, whose optical path length may exceed the coherent length. The speckle pattern is constructive or destructive by the moving RBCs within the image volume, which makes capturing the instantaneously motion of RBCs in capillaries with high resolution possible through the proposed ED-filtering of static tissue components.

## 3 Results

### 3.1 Quantification of RBCs Flow Velocity

Figures 2(a) and 2(b) show one representative raw speckle image and corresponding dynamic image of capillaries from a mouse ear. Figure 2(b) was obtained by the ED-filtering method, described in Sec. 2.1, from four raw speckle images, where the dynamic RBCs flow in the capillary are well extracted from strong static tissue signal. In Figs. 2(c) and 2(d), the solid, dotted, and dashed lines represent the time-varying raw and dynamic speckle signals observed at adjacent locations labeled with "A," "B," and "C" in Figs. 2(a) and 2(b), respectively. The peaks in the dynamic speckle signals indicate dynamic fluctuation due to the instantaneous moving RBCs within the imaging volume. Compared with the raw speckle signal, the

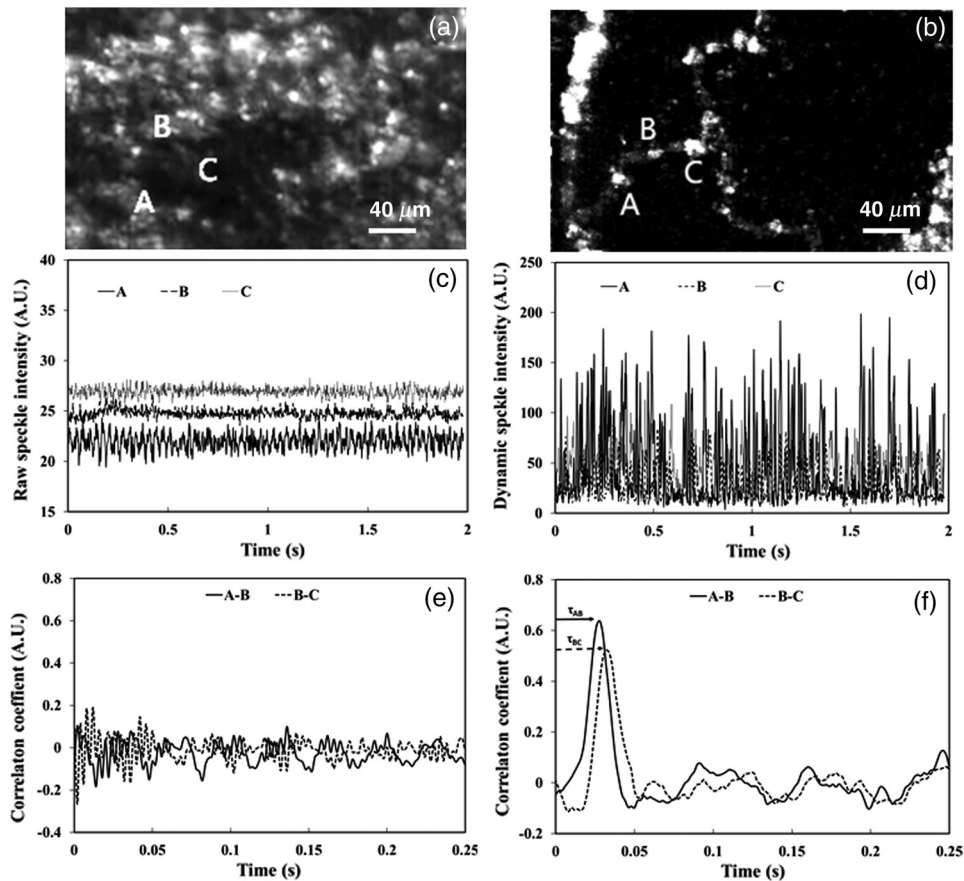


**Fig. 2** Quantification of RBCs flow velocity in single capillary. (a) Raw speckle image and (b) dynamic speckle mapping of RBCs flow. (c) Time-varying raw speckle signals and (d) dynamic speckle signals, observed at the locations labeled with “A,” “B,” “C” in (a) and (b), respectively. (e) Time-lagged cross-correlation functions of the raw speckle signals and (f) dynamic speckle signals, where “A-B” (“B-C”) denote the signal measured in A (B) and B (C), respectively.

RBCs flow in the dynamic speckle signal appears with high SNR due to the elimination of strong static tissue signal. The cross-correlation function of the dynamic speckle signals is shown in Fig. 2(f), while that of the raw speckle signals is shown in Fig. 2(e). It can be seen that there is hardly correlation between the raw speckle signals; however, a strong correlation between the extracted dynamic capillary signals is observed, but with a constant time delay of  $\tau_{AB}$  ( $\tau_{BC}$ ).  $\tau_{AB}$  ( $\tau_{BC}$ ) is related to the transit time of the RBC flow from the location of A (B) to B (C), respectively.

### 3.2 Velocity Measurements of Heterogeneous RBC Flow in Mouse Ear

The RBC flows in capillaries play an important role in maintaining the proper function of microcirculatory tissue beds, through releasing required oxygen to the surrounding tissue in direct contact with the tissue. Quantifying the RBCs flow velocity and pattern is important for investing the mechanisms of blood flow regulation in the capillary bed. We selected 16 capillaries from the RBCs flow map of the mouse ear in Fig. 2(a) to quantify the temporal flow velocities. With the time-varying dynamic speckle signal captured within 2 s, the moving window along the time dimension is 120 ms in width and 20 ms interval between successive windows, leading to 20 ms resolution for the temporal RBCs flow velocity distribution. The result is provided in Fig. 2(b). It is clear that the RBC flows in the capillaries

are highly heterogeneous in both temporal and spatial dimensions. The RBC flows with slower velocity [such as nos. 3 and 12 capillaries shown in Fig. 3(b)] appear more discrete with more “gap” between RBCs. The heterogeneous RBC flows are also related to slower perfusion and nonfully active capillaries under normal physiological state.

From a supplementary movie (Video 1), the dynamic speckle signal contains rich information about the RBC flow pattern. The correlated fluctuation patterns between neighboring locations indicate that RBCs moved in an ordered fashion in the capillaries. However, the dynamic speckle signals are less fluctuated in the main vessel branches because the RBCs in there assemble like clusters and travel faster, requiring much a faster sampling rate than that currently used in this study to maintain the signal fidelity. Due to this reason, the current system setup is more applicable to measuring slow and heterogeneous RBC flows in the capillaries. The higher resolution and dynamic range are possible to achieve through proper selections of exposure time of the camera, sampling rate, and microscopic magnification.

### 3.3 Quantitating Microcirculation Pattern Changes with Body Temperature

Quantitating the RBC flow changes under different physiological states provides additional information for understanding the mechanism of microcirculation regulation. We monitored the microcirculation response to the changes in body temperature,

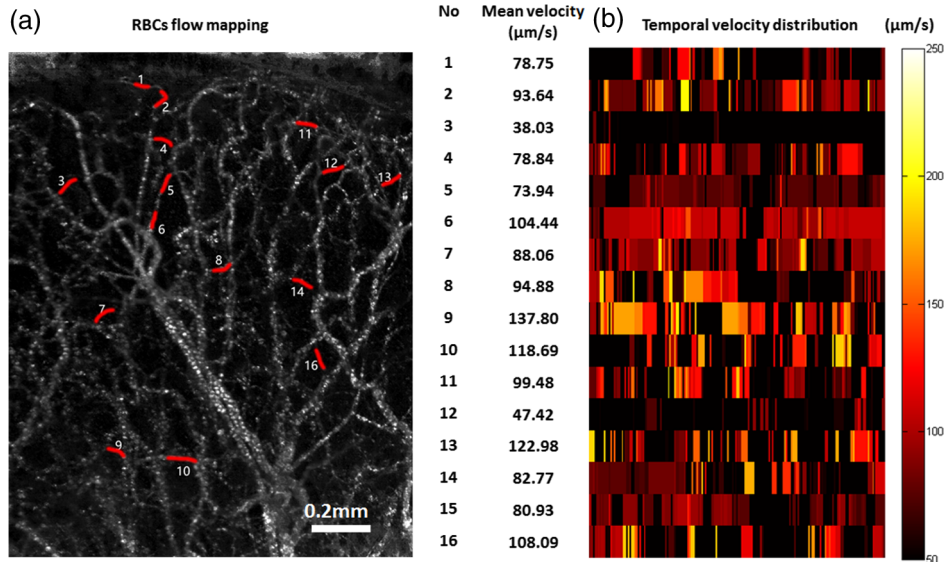


**Fig. 3** (a) Full-field RBC flow mapping of *in vivo* mouse pinna (b) Temporal velocity distribution of RBC flow in 16 capillaries in mouse pinna as shown in (a). (Video 1, MP4, 10.7 MB [URL: <http://dx.doi.org/10.1117/1.JBO.22.4.046002.1>]).

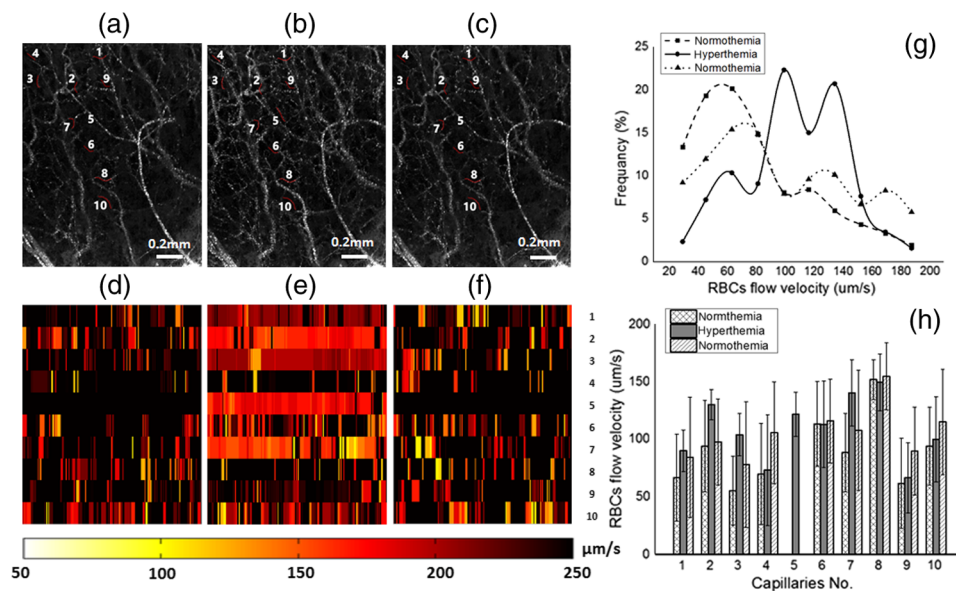


**Fig. 4** Full-field RBC flow mappings of *in vivo* mouse pinna with (a) normothermia, (b) hyperthermia, and (c) returning to normothermia. Temporal velocity distribution of RBCs flow in 11 capillaries with (d) normothermia, (e) hyperthermia, and (f) returning back to normothermia. The statistical results of the RBC flow velocity response to the thermoregulatory challenge are shown in (g) the frequency distribution and (h) the mean value and standard derivation of RBC flow velocity in single capillaries.

in an attempt to assert the sensitivity of the proposed approach to the changes in RBC flow pattern in capillaries. Figures 4(a)–4(c) show a series of full-field dynamic RBC flow images of the *in vivo* mouse pinna under the conditions of normothermia, hyperthermia, and returning back to normothermia (after hyperthermia), respectively. The increase of the body temperature leads to the increase of the capillary vessel density of the regions in between larger vessels. Some of the reserved capillaries are seen activated, demonstrating the increase of RBC flow and perfusion in the capillary beds. With the body temperature returning back to normothermia, the capillary vessel density returns to the normal level. Some of the reserved capillaries disappear in the

image, as shown in Fig. 4(c), indicating that the flows in those capillaries are no longer needed.

A total of 11 capillaries were chosen to quantify the changes of RBC flow velocities and patterns between normothermia and hyperthermia. As shown in Fig. 4(d), the slow and heterogeneous RBC flow suggests that many capillaries are not maximally utilized in a normal physiological state. With hyperthermia, the RBC flow becomes faster and more homogeneous in most capillaries, leading to high perfusion and efficient oxygen delivery. Meanwhile, some reserved capillaries also became functional [such as no. 5 capillary in Fig. 4(e)]. These changes are also confirmed by the statistical analysis results

shown in Figs. 3(g) and 3(h). From frequency distributions of RBC flow velocity, most of the RBC flow is with low velocity under normothermia. With hyperthermia, the number of high-velocity RBCs increases, accompanied by a reduction in the number of low-velocity RBCs. As the body temperature returns to normal state, the RBC flow velocity also comes back to the baseline. The changes of RBC flow pattern in single capillaries are validated with statistical parameters of mean value and standard derivation of temporal velocity, which are related to the velocity and heterogeneity of RBC flow, respectively. As shown in Fig. 3(h), in most of the capillaries, hyperthermia derives the increase of the mean velocity but the decrease of the standard derivation, indicating that RBC flows become faster and try to homogenize. The opposite changes are observed in most of the capillaries when the body temperature return to normothermia. Our results are in good agreement with previous observations.<sup>16</sup> However, RBC flow responses to the temperature challenge are a multifactorial phenomenon and are complicated in nature.<sup>17</sup> In some other capillaries (such as nos. 4, 9, and 10), the RBC flow velocity does not change immediately with hyperthermia; however, they increase velocity when returning to normothermia. In capillaries (such as no. 8), which has faster RBC flow under normal physiological state, the RBC flow velocity and pattern remain stable with hyperthermia.

The current study applies a simple transmission mode to demonstrate the approach, but most of the clinical applications require reflection measurement. As the biotissue is strongly forward-scattering media, the spatial correlation of the dynamic speckle signals may deteriorate due to lower SNR of the reflected signal when imaging is performed in reflection mode. One way to mitigate this problem is to use a reference arm to facilitate the interference, so the SNR of reflected dynamic speckle signals is increased.<sup>18</sup> We anticipate that the proposed approach could be applied in ophthalmology to measure RBC flow of capillaries that are superficially localized within thin and translucent retinal structure. The RBC flows are also related to the capability of oxygen delivery and consumption in the capillary beds. With multiple light sources of different wavelengths, this approach could be applied to measure the velocity and oxygenation of single file RBC flow simultaneously.<sup>19</sup>

## 4 Summary

In conclusion, we have developed an approach to achieve full-field velocity measurements of heterogeneous RBC flows using time-varying dynamic speckle signals. The results of *in vivo* mouse pinna demonstrated two important features of this approach: (1) its full-field mapping capability and (2) its capability for quantifying the velocity and heterogeneity of RBC flow in capillaries. This technique is expected to be a promising tool for noninvasive investigation of RBC hemodynamics during complicated physiological conditions.

## Disclosures

Dr. Li and Dr. Wang have no disclosures.

## Acknowledgments

The study was supported in part by the National Heart and Lung Institute (R01HL093140); the National Natural Science Foundation of China (81401454); the International Postdoctoral Exchange Fellowship Program of China (20140066); and China Postdoctoral Science Foundation (2013M541174).

## References

1. J. Lee, W. Wu, and D. A. Boas, "Early capillary flux homogenization in response to neural activation," *J. Cereb. Blood Flow Metab.* **36**(2), 375–380 (2016).
2. L. Østergaard et al., "Cerebral small vessel disease: capillary pathways to stroke and cognitive decline," *J. Cereb. Blood Flow Metab.* **36**(2), 302–325 (2016).
3. K. S. Øye et al., "A novel method for mapping the heterogeneity in blood supply to normal and malignant tissues in the mouse dorsal window chamber," *Microvasc. Res.* **75**(2), 179–187 (2008).
4. M. Mentek et al., "Compact laser Doppler flowmeter fundus camera for the assessment of retinal blood perfusion in small animals," *PLoS One* **10**(7), e0134378 (2015).
5. V. J. Srinivasan et al., "Micro-heterogeneity of flow in a mouse model of chronic cerebral hypoperfusion revealed by longitudinal Doppler optical coherence tomography and angiography," *J. Cereb. Blood Flow Metab.* **35**(10), 1552–1560 (2015).
6. R. Zhang et al., "Structured-illumination photoacoustic Doppler flowmetry of axial flow in homogeneous scattering media," *Appl. Phys. Lett.* **103**(9), 094101 (2013).
7. W. S. Kamoun et al., "Simultaneous measurement of RBC velocity, flux, hematocrit and shear rate in vascular networks," *Nat. Methods* **7**(8), 655–660 (2010).
8. D. A. Nelson et al., "High-resolution wide-field imaging of perfused capillaries without the use of contrast agent," *Clin. Ophthalmol.* **5**, 1095–1106 (2011).
9. A. Fercher and J. D. Briers, "Flow visualization by means of single-exposure speckle photography," *Opt. Commun.* **37**(5), 326–330 (1981).
10. J. Liang et al., "Cross-correlation-based transverse flow measurements using optical resolution photoacoustic microscopy with a digital micro-mirror device," *J. Biomed. Opt.* **18**(9), 096004 (2013).
11. Y. Wang and R. Wang, "Autocorrelation optical coherence tomography for mapping transverse particle-flow velocity," *Opt. Lett.* **35**(21), 3538–3540 (2010).
12. C. Li and R. Wang, "Dynamic laser speckle angiography achieved by eigen-decomposition filtering," *J. Biophotonics* (2016).
13. R. J. Harris, *A Primer of Multivariate Statistics*, Psychology Press, New York (2001).
14. C. Demeñé et al., "Spatiotemporal clutter filtering of ultrafast ultrasound data highly increases Doppler and ultrasound sensitivity," *IEEE Trans. Med. Imag.* **34**(11), 2271–2285 (2015).
15. D. Briers et al., "Laser speckle contrast imaging: theoretical and practical limitations," *J. Biomed. Opt.* **18**(6), 066018 (2013).
16. S. Yousefi, J. Qin, and R. K. Wang, "Super-resolution spectral estimation of optical micro-angiography for quantifying blood flow within microcirculatory tissue beds *in vivo*," *Biomed. Opt. Express* **4**(7), 1214–1228 (2013).
17. D. Kellogg, "In vivo mechanisms of cutaneous vasodilation and vasoconstriction in humans during thermoregulatory challenges," *J. Appl. Physiol.* **100**(5), 1709–1718 (2006).
18. Y. Wang, Z. Ma, and R. Wang, "Mapping transverse velocity of particles in capillary vessels by time-varying laser speckle through perturbation analyses," *Opt. Lett.* **40**(9), 1896–1899 (2015).
19. J. Qin et al., "Fast synchronized dual-wavelength laser speckle imaging system for monitoring hemodynamic changes in a stroke mouse model," *Opt. Lett.* **37**(19), 4005–4007 (2012).